

# A SPECTROSCOPIC STUDY OF A DECAYING HYDROGEN PLASMA

By F. E. IRONS\* and D. D. MILLAR\*

[Manuscript received May 19, 1964]

## Summary

A study has been made of the decay of a hydrogen plasma of ion density  $\sim 3 \times 10^{15} \text{ cm}^{-3}$  and temperature  $\sim 10^4 \text{ }^\circ\text{K}$ . Details are presented of the experimental methods used to determine density and temperature distributions in the decaying plasma. The plasma decays by three-body recombination mainly and the experimental values of the recombination coefficient agree with those expected for a plasma opaque to Lyman radiation.

## I. INTRODUCTION

Experimental observations of the decay of high density, low temperature plasmas have required values of the recombination coefficient of some 10 times the values expected for two-body (radiative) recombination. (For a review, see Bates and Dalgano 1962.) It is now known that these high values are caused by the three-body (electron-electron-ion) recombination process. Collisional-radiative recombination coefficients (three-body plus two-body) have been estimated by Byron, Stabler, and Bortz (1962) and by Hinnov and Hirschberg (1962) for an optically thin plasma. These agree with the more detailed calculations of Bates, Kingston, and McWhirter (1962), who also consider the case, which is relevant to the present work, of a plasma optically thick to lines of the Lyman series.

The object of the present paper is to describe the spectroscopic techniques that have been used to determine the time dependence of the distributions of ion density and electron temperature. From this has been obtained the recombination coefficient  $\gamma(N_e, T_e)$  defined by the relation  $dN_i/dt = -\gamma N_e N_i$ .

The spectrum of the plasma is a recombination spectrum. The lines of the Balmer series are strongly broadened by electron impacts and the interatomic electric fields—the Stark effect. This Stark broadening of the  $H\beta$ ,  $H\gamma$ , and  $H\delta$  lines has been used in the present work to measure the ion density  $N_i$  (equal to the electron density  $N_e$ ). The theory of Stark broadening in high density plasmas has been developed by Griem, Kolb, and Shen (1959, 1960, 1962) and the Stark profiles calculated by these authors have been verified experimentally in work with arcs and shock tubes (for a review see Baranger 1962). Above a density of around  $4 \times 10^{14} \text{ cm}^{-3}$  the Stark effect provides the most reliable measure of ion density.

The electron kinetic temperature  $T_e$  is that temperature which characterizes the Maxwellian distribution of electron velocities. For plasmas such as we are here considering a Maxwellian distribution should be established within  $1 \mu\text{s}$ . To determine  $T_e$ , use is made of the fact that the intensity  $I_\nu$  of an emission line is proportional

\* School of Physics, University of Sydney.

to the population density  $N_n(T_e)$  of the excited state of principal quantum number  $n$  from which the line originates. That is,

$$I_\nu = N_n A h \nu \text{ erg cm}^{-3} \text{ s}^{-1}, \quad (1)$$

where  $A$  is the transition probability. Furthermore, for  $n \geq 5$ , the population densities of the excited states are related to each other by the Boltzmann equation, and to  $T_e$  and  $N_e$  by the Saha equation (equation (2) below). A brief discussion of the recombination process, following the authors quoted in the opening paragraph, will explain the restriction to higher  $n$  values.

Initially the highly ionized plasma undergoes three-body recombination to the upper atomic levels predominantly, the rate varying as  $n^4$ . A balance is quickly established between this process and the inverse process of collisional ionization:



where  $\text{H}(n)$  denotes an atom excited to the level  $n$ .

Also important in establishing an equilibrium distribution among the upper levels and in extending the distribution down to the lower levels are the processes of collisional de-excitation and excitation:



The rates for these processes, mainly to adjacent states ( $n-m = \pm 1$ ), are very high for large  $n$  but decrease as  $n$  decreases, while the rate for (spontaneous) radiative de-excitation to all lower levels increases as  $n$  decreases. At  $n = 3$  for our plasma the two rates for de-excitation are approximately equal and, furthermore, the combined radiative plus collisional rate is a minimum. This means that the rate of depopulation of this level effectively determines the rate of recombination. The combined rate for the transition  $3 \rightarrow 2$  is greater than the rate for  $2 \rightarrow 3$  (collisional) so that, in general, electrons which pass through level  $n = 3$  proceed to the ground state. The rate of populating the ground state may be slowed if there is absorption of the Lyman radiation.

The population densities of levels  $n = 2$  and  $3$  quickly attain values which are steady but are below the equilibrium values. The population density of  $n = 4$  is expected to be more than 90% of its equilibrium value (Bates and Kingston 1963), while the levels  $n \geq 5$  are in equilibrium as a result of the processes (a) and (b).

The methods used for determining the temperature  $T_e$  from the intensities of emission lines and also from the intensity of the continuum are discussed below.

## II. EXPERIMENTAL APPARATUS

### (a) Plasma Preparation

A schematic drawing of Supper I, in which the plasma was prepared, is shown in Figure 1. This machine has been described in detail by Brennan, Lehane, *et al.* (1963). The plasma is prepared in a copper cylinder sealed at both ends by glass plates and situated in an axial magnetic field of up to 10 kG. By switching on a condenser bank to a central electrode mounted on one of the glass end plates an

ionizing front is initiated which propagates along the tube (Wilcox, Boley, and De Silva 1960; Wilcox, Baker, *et al.* 1962; Brennan, Brown, *et al.* 1963). Behind the front the plasma is left highly ionized and rotating. This rotation is removed by shorting the central electrode to the vessel wall ("crowbarring"). The plasma was prepared under the following conditions: hydrogen pressure = 100 millitorr; ionizing current = 7 kA; axial magnetic field = 10 kG; time of crowbar = 19  $\mu$ s after switch-on, i.e. 2  $\mu$ s less than the time required for the front to traverse the total length of Supper I.

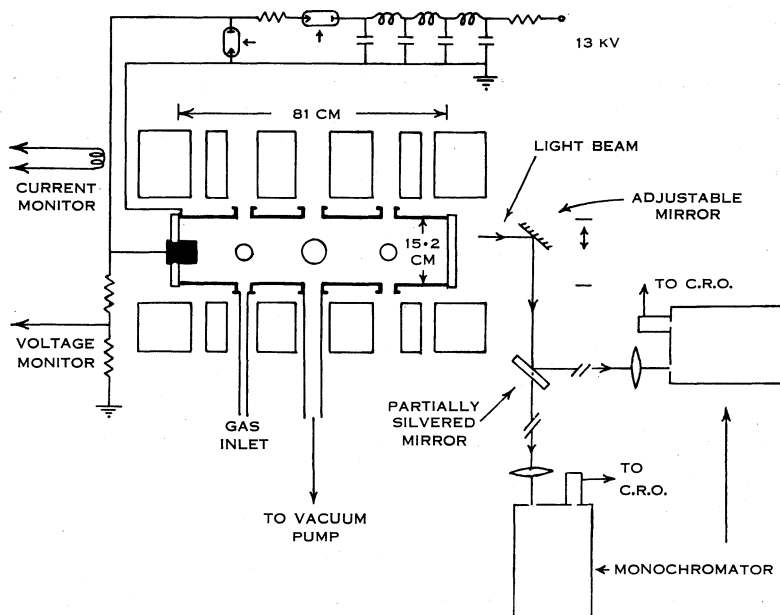


Fig. 1.—Schematic drawing of Supper I, showing the copper tube, the magnetic field coils, the plasma preparation condenser bank, and the two monochromators with their associated optics.

### (b) Spectroscopic

To measure the Stark profiles and the line intensities two Jarrell Ash monochromators were used of focal length 50 cm, aperture  $f/8.5$  and dispersion  $16 \text{ \AA}/\text{mm}$ . The Stark profile of  $H\beta$  at a density of  $6 \times 10^{14} \text{ cm}^{-3}$  has a half-width of  $1.4 \text{ \AA}$ . To measure profiles down to this half-width  $25\text{-}\mu\text{m}$  slits were used. For these slits the instrumental profile has a half-width of  $0.40 \text{ \AA}$ , for which allowance must be made. The instrumental profile was determined by scanning with the monochromator over a narrow line (Cd 4086) at a uniform, known speed and displaying the photomultiplier output on an oscilloscope. An E.M.I. 9536 photomultiplier in a Mumetal shield monitored the output from the monochromator. The signal from this passed through a cathode follower and was displayed on a Tektronix type 551 oscilloscope. The output signal above which the response of the system was non-linear was determined and subsequently never exceeded.

The measurements were made from the end of Supper I, and when both monochromators were in use the arrangement of Figure 1 was used. A beam of light was selected from various radial positions across the tube by means of stops and a movable mirror and was directed on to the entrance slits of the two monochromators by a half-silvered mirror and focusing lenses. The radius of the copper vessel was 7.5 cm and measurements were made at six positions spaced 1.25 cm apart between the centre and the wall.

An independent experiment showed that the monochromator responded equally to light from all distances along the line of sight, the inverse square fall-off in intensity being compensated by the increase in cross-sectional area of the field of view.

A calibration of the complete optical system, in situ, was made with a tungsten ribbon lamp.\* The calibration was repeated several times over a period of weeks with three different lamps and variations of  $\pm 3\%$  were noted. This was taken as an indication of the error in the calibration of the system (a relative calibration only was required).

### III. EXPERIMENTAL OBSERVATIONS

#### (a) *Spectrum Analysis*

The spectrum of the plasma was photographed using a small Hilger prism spectrograph. It showed, apart from the lines of the Balmer series, impurity lines from Na I, Si II and III, and C II. By crowbarring the plasma before the ionizing front hit the glass plate at the end of the machine the intensity of these lines was considerably reduced. The impurity level was considered too low to affect the behaviour of the plasma.

#### (b) *Framing Camera*

Framing camera photographs taken from the end of Supper I are shown in Figure 2. They give an indication of the gross behaviour of the plasma. The machine was fired many times to obtain the sequence shown and, because of the varying apertures used, the intensities of the photographs cannot be directly compared. The "swirls" produced by the action of the crowbar on the rotating plasma are similar to those reported by Wilcox, Cooper, *et al.* (1962) for a similar plasma. Both plasmas show a "hole" along the axis at early times. However, by 100  $\mu\text{s}$ , the present plasma has been induced to cross the magnetic field lines and the hole has filled in; this must be associated with the action of the crowbar since it does not occur without crowbar. By 140  $\mu\text{s}$  the plasma is uniformly bright across the tube except for the region near the wall where the plasma is already decaying rapidly. This boundary region of enhanced decay moves in towards the centre of the machine as the plasma is quenched.

#### (c) *Density and Temperature Measurements*

In order to study the plasma decay, the time variation of the radial distributions of density and temperature must be known. It was not possible to use the Abel

\* We are indebted to the National Standards Laboratory, CSIRO, Sydney, for the calibration of these lamps.

technique, since a side window covering the width of the vessel was not available. However, measurements at the three side ports shown in Figure 1 disclosed that

PLASMA PREPARATION  
 $J \times B$  FIRED POSITIVELY  
 CROWBAR AT  $19 \mu s$   
 PRESSURE 100 MTORR  
 MAGNETIC FIELD 10 KG

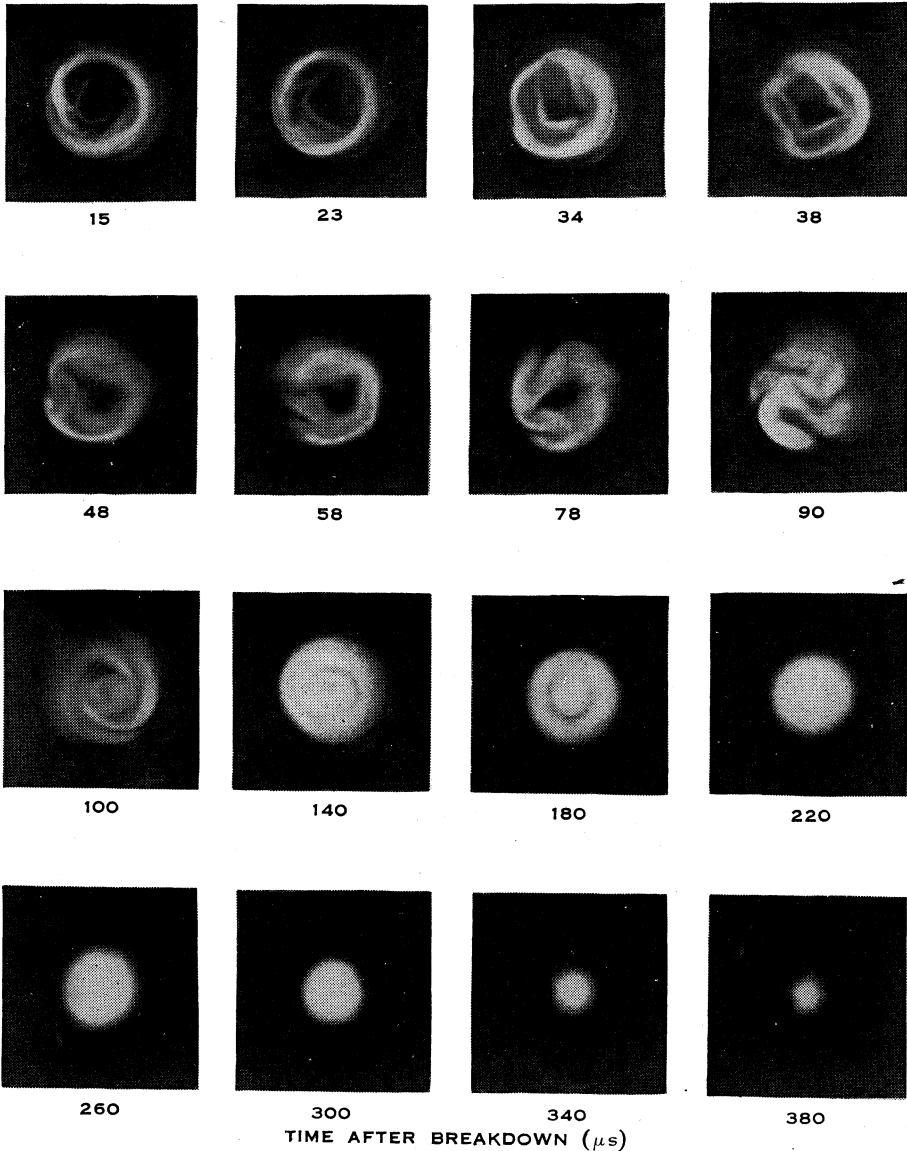


Fig. 2.—Framing camera photographs showing the decay of the plasma. Exposure time =  $0.1 \mu s$  up to  $T = 100 \mu s$  and  $1 \mu s$  thereafter.

the average densities and temperatures at these three ports were in agreement to within 10% and they showed no evidence for the development of longitudinal

density or temperature gradients. This fact justified the making of measurements from the end of the tube and removed a possible source of ambiguity from their interpretation.

(i) *Determination of Electron Density.*—The ion (= electron) density was determined from the Stark-broadened profiles of the  $H\beta$ ,  $H\gamma$ , and  $H\delta$  lines. The theoretical Stark profiles of  $H\gamma$  and  $H\delta$  have been presented in graphical form by Griem, Kolb, and Shen (1960), while the most recent calculations for  $H\beta$  are tabulated by Griem, Kolb, and Shen (1962). These calculations are independent of any assumptions concerning equilibrium distributions and are expected by the authors to be accurate to within 10%, an expectation which has been confirmed by experimental observations with arcs and shock tubes. The Stark-broadening method has the great merit that it is only weakly dependent upon the temperature and, to determine the density, the temperature need not be specified more accurately than to within  $\pm 50\%$ . The Stark profiles for  $T_e = 10^4$ °K have been used in the present work.

Because of these considerations it was not considered necessary to support the Stark method by an independent method such as the measurement of the absolute intensity of the continuum. However, the continuum at  $\lambda = 5094$  Å is only weakly dependent on  $T_e$  (for  $T_e > 8000$ °K) and the variation of this continuum intensity gives a good measure of the relative variation of  $N_e^2$ . This was found to be in good agreement with the relative variation of  $N_e^2$  with  $N_e$  determined from the Stark effect.

The Stark-broadened lines were treated by two different methods to yield the density. In the first the experimental profiles were compared with the theoretical profiles. In the second the density was determined from the measured ratio of the intensity of a small wavelength band at the line centre to the total line intensity. This latter method has also been used by Griem, Kolb, Lupton, and Phillips (1962).

(1) *Method 1.*—By interpolating between tabulated profiles a family of profiles was calculated and plotted with logarithmic ordinates at density intervals of  $1 \times 10^{14}$  cm<sup>-3</sup> up to  $1 \times 10^{15}$  cm<sup>-3</sup>, and of  $1 \times 10^{15}$  cm<sup>-3</sup> above this density. The experimental profiles were similarly plotted, and comparison with the theoretical profiles was done visually by superposing one on the other. The line wings (from 1/3 to 1/30 of the central line intensity) are the most sensitive parts of the line to changes in density and the points recorded in this region have the greatest influence on the assignment of a density. Only the far line wings had to be corrected for the continuum contribution.

In order to overcome the shot-to-shot fluctuations of 20% which occur when determining a line profile, point by point, with one monochromator, some 40–60 shots are necessary. This number may be reduced by using a second monochromator to continuously monitor one wavelength (chosen to be the line centre) and plotting the intensity at other wavelengths relative to the intensity of the monitor. The causes of the shot-to-shot variations are fluctuations in the neutral gas pressure ( $\pm 3\%$ ), in the ionizing current ( $\pm 3\%$ ), and in the magnetic field ( $\pm 5\%$ ). Any shot for which the monitor departed by more than about 30% from its average response was repeated, and if, during the course of a run, the monitor showed a

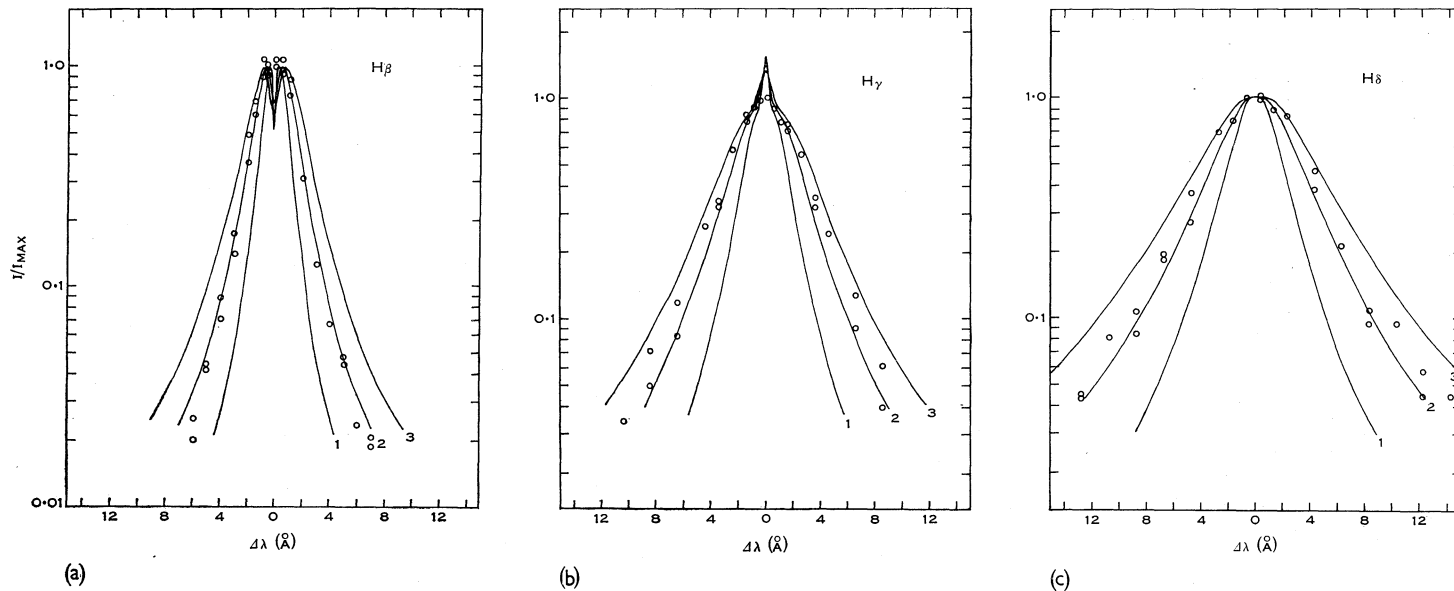


Fig. 3.—Experimental profiles (○) of  $H\beta$ ,  $H\gamma$ , and  $H\delta$  fitted against the theoretical Stark profiles. The densities assigned from these profiles are:  
 (a)  $H\beta$ ,  $N_e = (1.9 \pm 0.1) \times 10^{15} \text{ cm}^{-3}$ ; (b)  $H\gamma$ ,  $N_e = (2.3 \pm 0.3) \times 10^{15} \text{ cm}^{-3}$ ; (c)  $H\delta$ ,  $N_e = (2.2 \pm 0.2) \times 10^{15} \text{ cm}^{-3}$ .

drift, the cause was located and the run started anew. In this way good line profiles could be obtained by scanning the line once at some 15–20 wavelength settings. The line was then re-scanned at some 6–10 wavelengths to check further for consistency over the period of the run. In this way a complete Stark profile of a line could be established in about 40 min.

The profiles obtained in this way with two monochromators gave the same value of, and uncertainty in, density as did the profiles determined with one monochromator and a greater number of shots. Some typical profiles are shown in Figure 3. The uncertainty in density caused by the spread of the experimental points is typically  $\pm 0.2$  to  $0.3 \times 10^{15} \text{ cm}^{-3}$ .

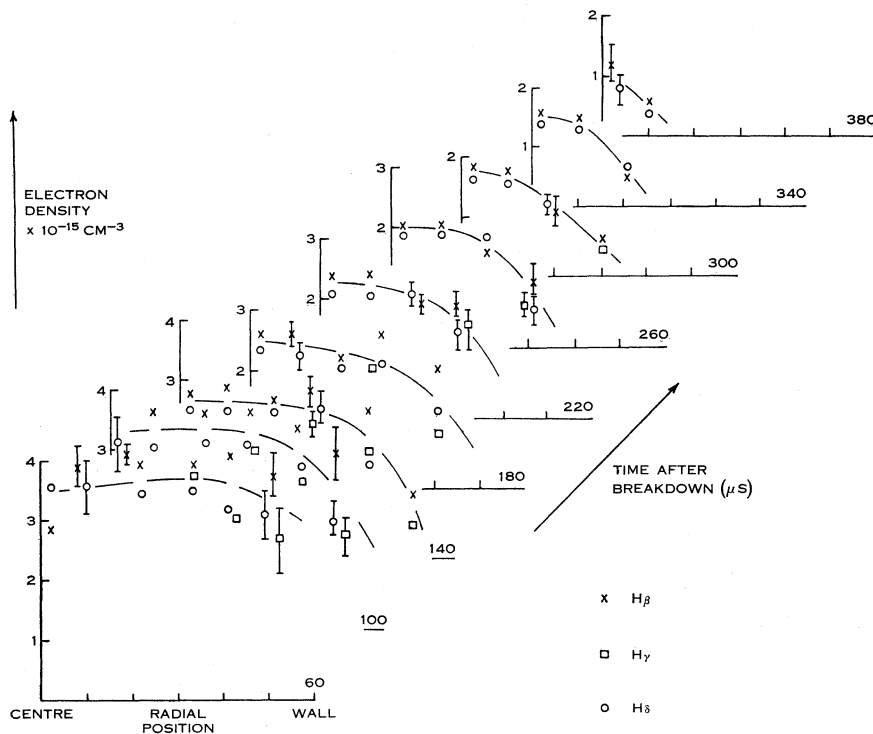


Fig. 4.—The variation of the radial electron density distribution with time.

This method was used to determine the radial density distributions shown in Figure 4. Measurements of the  $H\beta$  and  $H\delta$  lines were made at all six radial positions, and on  $H\gamma$  only near the wall. In the central region of the vessel, where the density was uniform, the two values of the density were consistent. Near the wall, where the density and temperature were both changing rapidly in space and time, the shot-to-shot variation was large, and this was reflected in the differences of up to 40% between the three values of density.

(2) *Method 2.*—The ratio of the intensity of the light from a small wavelength interval,  $\Delta\lambda$ , centred on the line centre, to the total line intensity may be calculated

from the theoretical Stark profiles and this ratio may then be used as a measure of the ion density. The value of  $\Delta\lambda$  will depend upon the density range of interest. For the line  $H\beta$  a choice of  $\Delta\lambda = 2.1 \text{ \AA}$  (130- $\mu\text{m}$  exit slit on the monochromator) makes the ratio sensitive to densities in the range 1 to  $5 \times 10^{15} \text{ cm}^{-3}$ , as shown in Figure 5. To record the density on a single shot, two monochromators were used as in Figure 1, one recording the line centre, the other the total line intensity. A single monochromator has since been modified to carry out this measurement alone using a beam-splitting, half-silvered mirror to direct light within the monochromator on to a second exit slit and photomultiplier tube mounted on the side of the instrument.

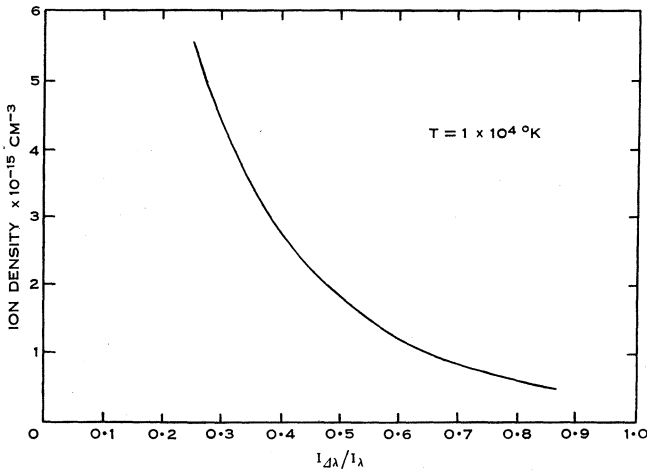


Fig. 5.—The ratio  $I_{\Delta\lambda}/I_{\lambda}$  for  $H\beta$ , with  $\Delta\lambda = 2.1 \text{ \AA}$ , as a function of  $N_e$ .

The mean spread in density from shot to shot as measured by this technique was the same as the uncertainty in density using method 1. Once the monochromator has been set with the line centre correctly imaged on the exit slit this method can give densities from a single shot. Only a small correction need be made for the background continuum radiation and corrections for instrumental and Doppler effects are similar to those for method 1 (see below).

The radial density profiles taken with an axial magnetic field of 6 and 8 kG (not shown here) were determined by this method.

(3) *Line broadening corrections.*—The effects of Doppler and instrumental broadening (of half-widths 0.35 and 0.40  $\text{\AA}$  respectively) are too small to alter the Stark character of the lines but they do contribute slightly to the broadening. The three processes are independent and consequently their effects can be folded in together; for this Voigt functions were used (van de Hulst and Reesinck 1947). When this was done and the resulting profiles compared with the theoretical Stark profiles, it was found that for  $H\beta$  the effect of the Doppler and instrumental broadening was to give a higher density by an amount  $\Delta N = 2 \times 10^{14} \text{ cm}^{-3}$ , constant to within

20%, throughout the density range  $6 \times 10^{14}$  to  $5 \times 10^{15}$  cm $^{-3}$ . For H $\gamma$ ,  $\Delta N = 1.5 \times 10^{14}$  cm $^{-3}$  and for H $\delta$ ,  $\Delta N = 1 \times 10^{14}$  cm $^{-3}$ . The correction for Doppler and instrumental broadening was then made by subtracting the appropriate value of  $\Delta N$  from the density determined from the experimental profile using both methods 1 and 2.

(ii) *Determination of Electron Temperature.*—The electron temperature was determined by three separate methods:

(i) from the ratio of the intensities of two bands of the continuum, one in the visible, the other in the ultraviolet (Balmer continuum),

(ii) from the ratio of the intensities of an emission line to a band of the continuum.

Provided the continuum is produced only by the H atom (see below) the ratios of (i) and (ii) are independent of electron density.

(iii) from the Balmer decrement. This is independent of electron density but is insensitive to temperatures above about 10 000°K in the present application.

(1) *Emission lines.*—In the introduction it was pointed out that the atomic states with  $n \geq 5$  may be expected to have attained their equilibrium population densities  $N_n$ . These are related to the electron and ion densities,  $N_e$  and  $N_i$  respectively, by the Saha equation:

$$N_n = N_e N_i \frac{h^3 n^2}{(2\pi m k T_e)^{3/2}} \exp(\nu_n - \Delta I)/k T_e, \quad (2)$$

where  $h\nu_n = 13.6/n^2$  eV and  $\Delta I$  is the reduction in the ionization potential caused by the electric fields within the plasma (Griem 1962). It is negligible for our plasma and in any case the term drops out when ratios as in (i) and (ii) are taken.

The equations (1) and (2) then relate the Balmer line intensity to the density and temperature. The line H $\gamma$  ( $n = 5 \rightarrow 2$ ) was chosen for the temperature measurements since it has a stronger temperature dependence than any higher series line.

(2) *The continuum.*—The calculation of the continuum intensity is not dependent upon there being equilibrium, but only upon the assumption of a Maxwellian distribution of electron velocities. For this reason the continuum should provide the most reliable measure of temperature, except that it is a weak function of temperature.

The continuum is composed of the free-bound and free-free continuum of the H atom and the H $^-$  ion. The transitions are:

$$\begin{array}{l} \text{H atom} \\ \text{H}^- \text{ ion} \end{array} \left\{ \begin{array}{l} \text{free-bound } \text{H}^+ + e \rightarrow \text{H}(n) + h\nu \quad (75\%), \\ \text{free-free } \text{H}^+ + e + \text{KE} \rightarrow \text{H}^+ + e + h\nu \quad (12\%), \\ \text{free-bound } \text{H} + e \rightarrow \text{H}^- + h\nu \quad (11\%), \\ \text{free-free } \text{H}^- + e + \text{KE} \rightarrow \text{H}^- + e + h\nu \quad (2\%). \end{array} \right.$$

The brackets contain the contribution of each process to the total continuum when  $\lambda = 5094$  Å,  $T_e = 10\,000^\circ\text{K}$ ,  $N_e = 2.0 \times 10^{15}$  cm $^{-3}$ , and the neutral atom density in the ground state,  $N_0 = 4.6 \times 10^{15}$  cm $^{-3}$ .

The intensity of the H continuum per ångstrom wavelength interval is given by:

$$I_\lambda = 1.89 \times 10^{-29} \frac{N_i N_e}{(kT)^{1/2}} \exp(-h\nu/kT) (10^4/\lambda)^2 \exp(-\Delta I/kT) \times$$

$$\times \left( g_{ff} + \frac{2I}{kT} \sum_{n \geq 2}^{\infty} \frac{g_{fb} \exp(h\nu_n/kT)}{n^3} \right) \text{ erg cm}^{-3} \text{ s}^{-3}, \quad (3)$$

where  $\lambda$  is in ångstroms,  $kT$  in eV,  $I = 13.6$  eV,  $h\nu_n = 13.6/n^2$ . The  $g$ -factors are the quantum mechanical Gaunt factors ( $\sim 1$ ). The first term in the bracket gives the contribution from the free-free transitions and the second term the free-bound transitions. For  $n \geq 6$  the sum was evaluated by an integral approximation.

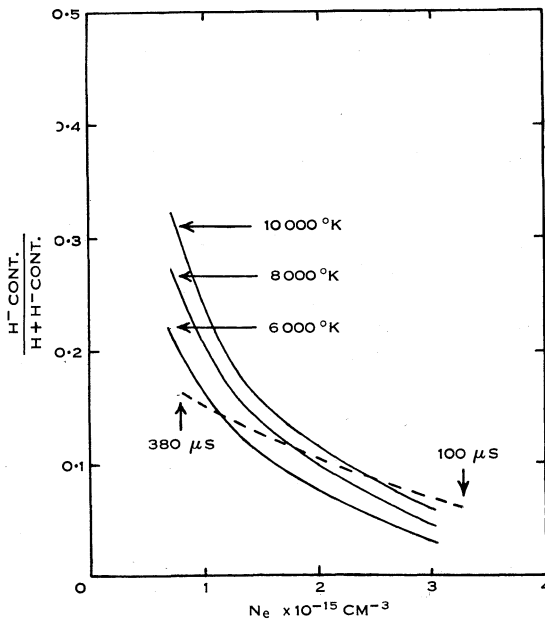


Fig. 6.—The variation of  $\{H^- \text{ cont.}/(H+H^-) \text{ cont.}\}$  as a function of  $N_e$  and  $T_e$  for  $N_e+N_0 = 6.6 \times 10^{15} \text{ cm}^{-3}$ . The values taken by the present plasma are shown by the broken line.

The intensity of the  $H^-$  continuum cannot similarly be expressed in analytical form and has been calculated from tables of absorption coefficients presented by Chandrasekhar and Breen (1946) for the free-bound, and by Ohmura and Ohmura (1961) for the free-free transitions.

Note that the intensities of both  $H\gamma$  and the H atom continuum are proportional to the product  $N_e N_i$  and their ratio is independent of density. Unfortunately the intensity of the  $H^-$  continuum is proportional to the product  $N_e N_0$ , so that the relative contribution of  $H^-$  to the total continuum changes with  $N_e$  and  $N_0$  and also with  $T_e$ . In Figure 6 the ratio of the intensity of the  $H^-$  continuum to that of

the  $H+H^-$  continuum is shown as a function of  $N_e$  and  $T_e$ ;  $N_0$  is defined by assuming that  $N_0+N_e = 6.6 \times 10^{15} \text{ cm}^{-3}$ , the initial particle density for a pressure of 100 millitorr. This value of  $N_0$  is several orders of magnitude smaller than the value to be expected for the same value of  $N_e$  if the plasma were in local thermal equilibrium and the ratio  $\{H^- \text{ cont.}/(H+H^-) \text{ cont.}\}$  remains much smaller than might at first be expected. The values of this ratio for the values of  $N_e$  and  $T_e$  encountered in the present work are indicated by the dashed line of Figure 6. With these data the contribution of the  $H^-$  continuum can be subtracted from the measured continuum.

The continuum intensity was measured with a 32-Å pass band at two wavelengths, 5094 and 3440 Å. These are beyond the influence of the wings of the Balmer lines and in regions of the spectrum which were scanned and found to be free of impurity lines. Correction for the  $H^-$  ion contribution as described above was not necessary at 3440 Å since it contributes less than 1% to the total continuum.

For the remainder of this paper the H continuum at 5094 Å,  $I_\lambda d\lambda$  with  $d\lambda = 32 \text{ Å}$ , is denoted "cont. 5094" and is the observed continuum at this wavelength from which the  $H^-$  continuum has been subtracted.

(3) *Temperature from ratios of line and continuum intensities.*—For a given electron density the line and continuum intensities behave differently with temperature. As the temperature increases from 6000°K to 12 000°K the intensity of  $H\gamma$  drops rapidly, the continuum at 3440 Å decreases slowly, while the continuum at 5094 Å increases slowly. Consequently the ratio ( $H\gamma/\text{cont. 5094}$ ) is a strong function of temperature while ( $H\gamma/\text{cont. 3440}$ ) and ( $\text{cont. 3440}/\text{cont. 5094}$ ) are only moderate functions of temperature, as shown in Figure 7. The three ratios allow three determinations of temperature to be made. The values should be internally consistent and, in fact, of 37 measurements, in only 6 did the three temperatures differ by more than 20%.

(4) *The Balmer decrement.*—As previously noted, for the states  $n \geq 5$  collision processes determine the population of the atomic states and the excitation temperature should then be the same as the electron temperature. The decrement was determined from the relative intensities of the lines  $H\gamma$ ,  $H\delta$ ,  $H\epsilon$ , and  $H\zeta$ . Above  $H\zeta$  the lines start to merge. The energy difference between the levels 5 and 8 is only 0.32 eV and the term  $\exp(-0.32/kT_e)$ , which essentially determines the decrement, is only a weak function of temperature for  $T_e$  above about 10 000°K. At this temperature a variation of  $\pm 7\%$  in the intensity of the lines would result in a variation of  $\pm 20\%$  in temperature. Around 7000°K this variation in the temperature falls to  $\pm 5\%$ .

(5) *Measurements.*—The measurements were made with a single monochromator, setting on each wavelength region in turn. A 32-Å band of the continuum was measured, and for line intensities a 57-Å pass band was used. Six to nine shots were fired at each setting. The standard deviation was typically 5% and was approximately the same for lines and continuum. This, together with the estimated error in the calibration, leads to the following estimated uncertainty in measuring

a temperature of  $10\,000^\circ\text{K}$ :  $\pm 800^\circ$  from ( $\text{H}\gamma/\text{cont. 5094}$ ),  $\pm 1200^\circ$  from ( $\text{H}\gamma/\text{cont. 3440}$ ), and  $\pm 1100^\circ$  from ( $\text{cont. 3440}/\text{cont. 5094}$ ). The corresponding errors in the Balmer decrement method are indicated above.

The temperature distributions are shown in Figure 8. In general the different methods give results which are in agreement, but it does appear that above about

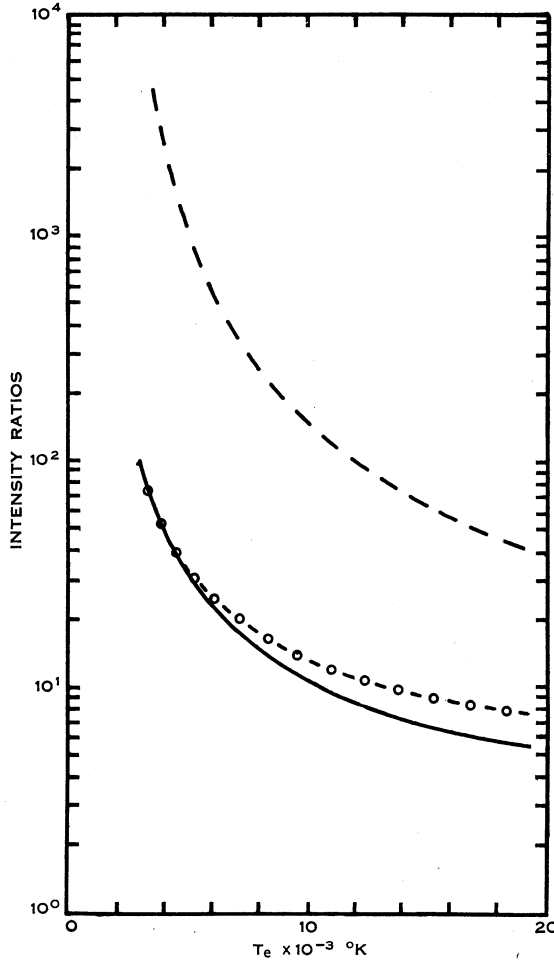


Fig. 7.—The ratios,  $\text{H}/(\text{cont. 5094})$ , — — —,  $\text{H}/(\text{cont. 3440})$  —  $\circ$  —  $\circ$ , and  $(\text{cont. 3440})/(\text{cont. 5094})$  — — —, as functions of  $T_e$ .

$8000^\circ\text{K}$  the Balmer temperatures are systematically lower than the others. This may be caused by errors in the calibration and in the corrections which were made for the continuum to the  $\text{H}\epsilon$  and  $\text{H}\zeta$  line intensities. The continuum could not be measured near these lines and was extrapolated from measurements made at higher wavelengths.

## IV. DISCUSSION

The radial distributions of electron density and temperature exhibit two striking features. Firstly, for a period of some 200  $\mu\text{s}$  the density and temperature remain uniform from the centre out to a fairly well defined radius where both then drop to about half of their central values within a distance of 2 cm. This behaviour was also observed in the radial distribution of the  $\text{H}\gamma$  light intensity, and is also shown in the framing camera photographs of Figure 2, in which the light is principally of the Balmer series. Secondly, as the plasma decays so the central, bright, high density and temperature plasma diminishes in its radial extent.

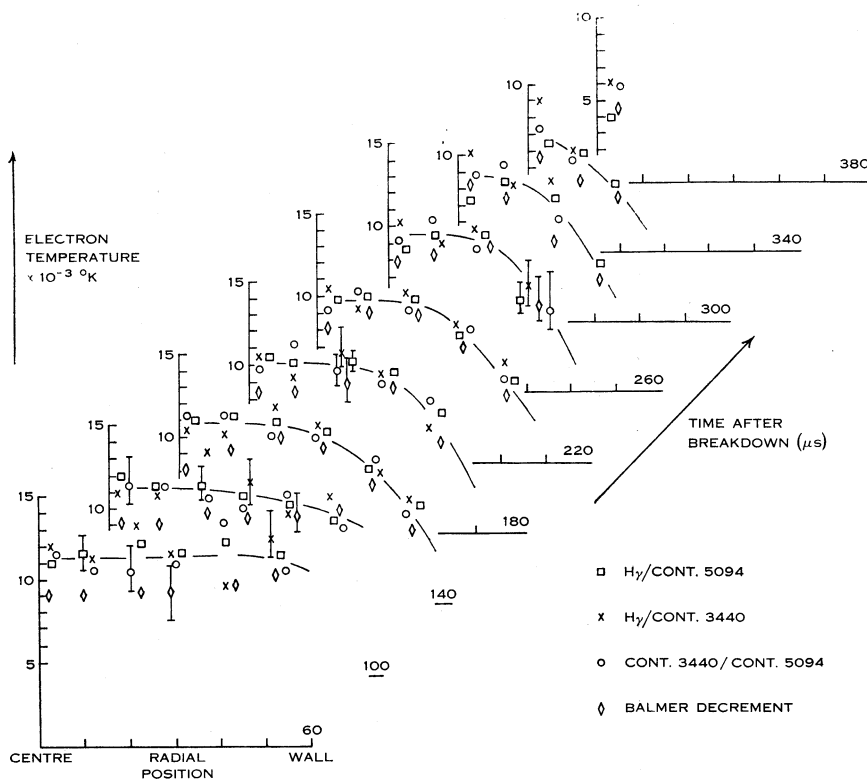


Fig. 8.—The variation of the radial electron temperature distribution with time.

Analysis of the plasma decay can be separated into two parts—(i) the decay of the central uniform plasma and (ii) the mechanism of energy loss from the plasma which determines the temperature.

Diffusion across the magnetic field of 10 kG is a slow process (Spitzer 1962) and, moreover, should vary as the square of the magnetic field. It was found that the characteristics of the plasma decay were little changed when the field was reduced to 6 kG.

(i) The calculations of Bates, Kingston, and McWhirter (1962) for the decay of a plasma by three-body and radiative recombination is applicable to the present

situation. The decay coefficient  $\gamma$  is proportional to  $N_e^a T_e^{-\beta}$ , with  $a$  and  $\beta$  approximately 1 and 4 respectively in the density and temperature range here considered. The values of  $\gamma$  deduced from the experimental observations on the axis of the tube are shown as a function of time in Figure 9. These values agree very closely with the values expected for a plasma opaque to Lyman radiation, and are  $\sim 10$  times smaller than the values for a plasma transparent to all radiation. The decay

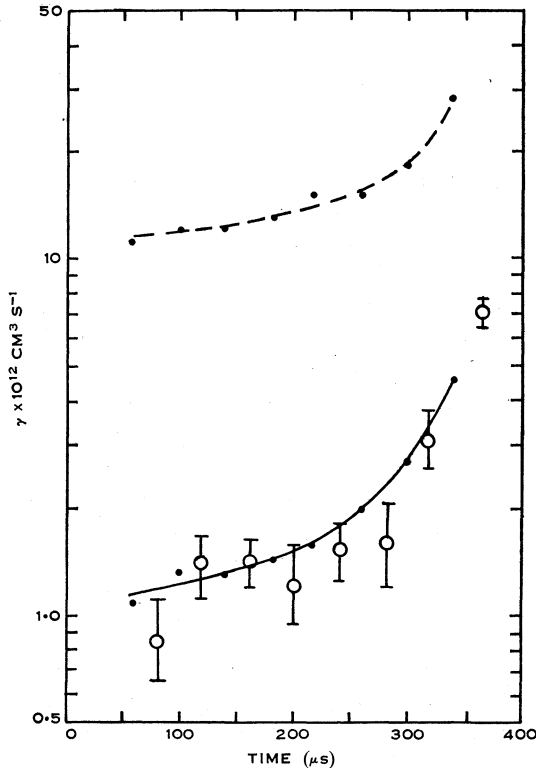


Fig. 9.—The variation of the decay coefficient  $\gamma$  as a function of time at the radial position  $r = 0$ . Also shown are the values of  $\gamma$  (Bates, Kingston, and McWhirter 1962) to be expected from the observed  $N_e$  and  $T_e$ , for the cases of a plasma (i) transparent to all optical radiation (---) and (ii) opaque to Lyman radiation (—).

of the central plasma density appears, then, to be adequately described by collisional-radiative recombination with complete absorption of Lyman radiation.

In the outer layer of plasma a marked temperature gradient exists. The strong temperature dependence of the recombination coefficient then affords a qualitative explanation for the coincidence of the electron density gradient and the electron temperature gradient which together define the boundary of the plasma.

(ii) The temperature distributions of Figure 8 are determined by the energy loss processes of radiation and thermal conductivity.

Because the plasma is collision-controlled there is a continuous interchange of energy between electron kinetic energy and ionization energy through the process (a) and further between the electron kinetic energy and the kinetic energy of ions and neutrals. Because of the short collision times (Spitzer 1962) electrons, ions, and neutrals may all be considered to have the same temperature  $T_e$ , and the internal energy per unit volume may be written as

$$E = \frac{3}{2}(N_e + N_i + N_0)kT_e + IN_i,$$

where  $I$  is the ionization energy. Assuming  $N_i + N_0$  to remain constant and equal to the initial neutral atom density of  $6.6 \times 10^{15} \text{ cm}^{-3}$ , the time-dependent measurements of  $N_e (= N_i)$  and of  $T_e$  determine  $dE/dt$ , the total power loss from the plasma. The radiant power loss for a plasma opaque to Lyman radiation may be derived from the tables of Bates and Kingston (1963); this accounts for about half of the total power loss. If the remainder is accounted for by thermal conductivity, the values of the coefficient of thermal conductivity are found to lie in the range of 1 to 4  $\text{J(m s deg)}^{-1}$ . In the outer, cool gas, where  $N_e$  and  $T_e$  are not measurable, the average temperature gradient between the hot plasma and the vessel wall is of the order of  $10^5 \text{ }^\circ\text{K m}^{-1}$  and a thermal conductivity coefficient of the order of 1  $\text{J(m s deg)}^{-1}$  again is found to account satisfactorily for the heat flux.

It is of interest to note that such values of the coefficient of thermal conductivity are close to those predicted for a neutral, monatomic hydrogen gas with geometric collision cross section. They are some 10 times larger than the value predicted for a fully ionized plasma at the same temperature of  $10^4 \text{ }^\circ\text{K}$  and several hundred times larger than the predicted value for a fully ionized plasma transverse to the magnetic field of 10 kG used in this experiment (Braginsky 1958; Spitzer 1962).

This would appear to indicate that it is the neutral atoms which transport the thermal flux out of the plasma to the vessel wall. However, it should be noted that the plasma may not be completely opaque to Lyman radiation and this introduces some uncertainty in the evaluation of the radiant power loss and hence in the above high estimate of the plasma thermal conductivity.

## V. ACKNOWLEDGMENTS

The authors are grateful to Professor C. N. Watson-Munro for discussion in the course of this work, also to Professor H. Messel for the provision of research facilities in the School of Physics and to several New South Wales manufacturers and to the Australian Institute of Nuclear Science and Engineering for financial support.

One of us (F.E.I.) acknowledges provision of a Research Studentship from the Australian Institute of Nuclear Science and Engineering.

## VI. REFERENCES

- BARANGER, M. (1962).—"Atomic and Molecular Processes." (Ed. D. R. Bates.) Ch. 13. (Academic Press: New York.)
- BATES, D. R., and DALGANO, A. (1962).—"Atomic and Molecular Processes." (Ed. D. R. Bates.) Ch. 7. (Academic Press: New York.)

- BATES, D. R., and KINGSTON, A. E. (1963).—*Planet. Space Sci.* **11**: 1.
- BATES, D. R., KINGSTON, A. E., and McWHIRTER, R. W. P. (1962).—*Proc. Roy. Soc. A* **267**: 297; **270**: 155.
- BRAGINSKY, S. J. (1958).—*J.E.T.P.* **6** (33): 358.
- BRENNAN, M. H., BROWN, I. G., MILLAR, D. D., and WATSON-MUNRO, C. N. (1963).—*J. Nuclear Energy C* **5**: 229.
- BRENNAN, M. H., LEHANE, J. C., MILLAR, D. D., and WATSON-MUNRO, C. N. (1963).—*Aust. J. Phys.* **16**: 340.
- BYRON, S., STABLER, R. C., and BORTZ, R. I. (1962).—*Phys. Rev. Letters* **8**: 376.
- CHANDRASEKHAR, S., and BREEN, F. H. (1946).—*Astrophys. J.* **104**: 430.
- GRIEM, H. R. (1962).—Proc. 5th Internat. Conf. on Ionization Phenomena in Gases. Vol. 2, p. 1857. (North Holland Publishing Co.: Amsterdam.)
- GRIEM, H. R., KOLB, A. C., LUPTON, W. R., and PHILLIPS, D. T. (1962).—*J. Plasma Phys., Thermonuclear Fusion Suppl.* (2): 543.
- GRIEM, H. R., KOLB, A. C., and SHEN, K. Y. (1959).—*Phys. Rev.* **116**: 4.
- GRIEM, H. R., KOLB, A. C., and SHEN, K. Y. (1960).—U.S. Naval Research Lab. Rep. 5455.
- GRIEM, H. R., KOLB, A. C., and SHEN, K. Y. (1962).—*Astrophys. J.* **135**: 272.
- HINNOV, E., and HIRSCHBERG, J. G. (1962).—*Phys. Rev.* **125**: 795.
- VAN DE HULST, H. C., and REESINCK, J. J. M. (1947).—*Astrophys. J.* **106**: 121.
- OHMURA, T., and OHMURA, H. (1961).—*Phys. Rev.* **121**: 513.
- SPITZER, L., JR. (1962).—"Physics of Fully Ionised Gases." Ch. 5. (Interscience: New York.)
- WILCOX, J. M., BAKER, W. R., BOLEY, F. I., COOPER, W. S., III, DE SILVA, A. W., and SPILLMAN, G. R. (1962).—*J. Nuclear Energy C* **4**: 337.
- WILCOX, J. M., BOLEY, F. I., and DE SILVA, A. W. (1960).—*Phys. Fluids* **3**: 15.
- WILCOX, J. M., COOPER, W. S., DE SILVA, A. W., SPILLMAN, G. R., and BOLEY, F. I. (1962).—*J. Appl. Phys.* **33**: 2714.

